Finite-Time Transport Structures of Flow Fields

Kuangyu Shi[*]   Holger Theisel[†]   Tino Weinkauf[‡]   Hans-Christian Hege[§]   Hans-Peter Seidel[¶]
MPI Informatik   Magdeburg University   Zuse Institute Berlin   Zuse Institute Berlin   MPI Informatik

ABSTRACT

Modern experimental and computational fluid mechanics are increasingly concerned with the structure nature of fluid motion. Recent research has highlighted the analysis of one transport structure which is called Lagrangian coherent structure. However, the quantity nature of the flow transport is still unclear. In this paper, we focus on the transport characteristics of *physical quantities* and propose an approach to visualize the finite-time transport structure of quantity advection. This is similar to an *integral convolution* over a scalar field along *path-lines* of a flow field. Applied to a well-chosen set of physical quantity fields this yields structures giving insights into the dynamical processes of the underlying flow. We demonstrate our approach on a number of test data sets.

Index Terms: I.3.8 [Computing Methodologies]: Computer Graphics—Applications;

1 INTRODUCTION

Transport is one dominant phenomenon during a flow process. It describes particles or quantities moving in a flow [15]. An effective visual analysis of flow transport is still a challenging problem in scientific visualization. Although a number of promising approaches have been introduced in recent years, it has still proved to be inherently difficult to actually comprehend the important characteristics of this complex dynamical phenomenon.

Classical approaches of dynamical analysis tend to extract the transport features in Eulerian perspective and to track these features along time. Features, such as physical quantities, trajectory topologies or vortex core lines, are extracted at a certain number of time steps. The correspondence of these features in consecutive time steps is detected and the coherency or evolution of these features is visualized. Though these approaches generate promising results, the extracted features depend strongly on each static step and they are not natural for dynamical analysis.

Advection is generally the major transport mode in a fluid which describes the transport by the macroscopic motion of currents in contrast to diffusion or radiation [4]. Any substance, or conserved quantity such as dye, momentum or heat can be advected in a fluid. For an advection process, a fluid is described mathematically as a vector field [16, 20]. In flow visualization, *Line integral convolution* (LIC) is one standard technique to approach the flow advection nature [5]. It is similar to advect a noise texture field along flow transport trajectories and generate the motion blur of the processing texture. This texture motion blur reflects the underling substance concentration which figures out the geometrical distribution of the corresponding trajectories [5, 27].

Lagrangian coherent structure (LCS) is one highlight in flow transport analysis which identifies the transport barriers during flow

[*]e-mail: skyshi@mpi-inf.mpg.de

[†]e-mail:theisel@isg.cs.uni-magdeburg.de

[‡]e-mail:weinkauf@zib.de

[§]e-mail:hege@zib.de

[¶]e-mail: hpseidel@mpi-inf.mpg.de

advection [11]. Recent research has characterized LCS with the attributes of finite-time particle trajectories (path-lines). A finite-time Lyapunov exponent (FTLE) field is computed to describe how much particles separate after a given interval of time. LCS is visualized from the ridges of the corresponding FTLE field. In contrast to traditional approaches, LCS gives a different and natural insight into the dynamical processes of flow transport. However, some important physical quantities are not considered and the advection characteristics of these quantities are still not clear. To get a better understanding of intrinsic flow transport, the visual analysis of physical quantity advection for a flow field is necessary. For this analysis, it is not enough to investigate only the trajectories. The corresponding physical quantities need to be included.

In this paper, we propose an approach of visualizing quantity transport behaviors using similar idea as LIC. Instead of a noise texture, our approach *convolutes* a correlated *physical quantity* field of interest along *path-lines*. This is similar to carry the physical quantities along flow transport and record the advection blur of these quantities. The result field of the convolution is different from the original physical quantity field, since it senses the dynamical behavior of the quantity and it distinguishes from the traditional LIC result while it captures the quantity characteristics of the flow field.

For a given focus time, we make a regular sampling in the spatial domain and from each sampled point, we start a convolution with some carefully-selected correlated physical quantity fields along integrated path-lines. Finite-time transport structures for physical quantities are identified by the result fields of the convolution over a certain time, which are analyzed and visualized through applying traditional scalar field visualization techniques. These structures identify the concentration nature of the quantity advection and present a significant different view to dynamical processes.

The rest of the paper is organized as follows. Section 2 mentions related works in visualization of dynamical flow transport. Section 3 recalls some ideas of flow transport visualization. Section 4 describes our approach to visualize the finite-time transport structures of quantity advection. Section 5 demonstrates our approach on a number of test data sets. Section 6 draws conclusions and discusses issues of future research.

2 RELATED WORKS

Many approaches have been introduced to explore dynamical flow behaviors. Traditional work focuses on tracking the features, such as topological features [35, 33, 9] and vortex regions [1, 2, 3, 32], in Eulerian perspective. Quantity features during the flow processes are typically visualized as time-varying data sets [19].

LIC, first introduced by Cabral and Leedom [5], has become one of the standard flow visualization techniques. Rezk-Salama et al. propose effective LIC extension to 3D flow visualization [22]. Shen et al. use LIC to synthesis dye advection in a flow to enhance local features [27]. Stalling and Hege present significant improvements in LIC performance by exploiting coherence along streamlines [30]. LIC has also been done with path-lines to deal with unsteady flow [26].

There has been much work done in analyzing LCS. Early work focuses on the study of uniformly hyperbolic path-lines [21]. Haller has pioneered the introduction of the FTLE field to characterize LCS [10, 14, 11]. He also proposed to identify stable and unstable manifolds with ridge lines of FTLE fields [12]. [25] provided a
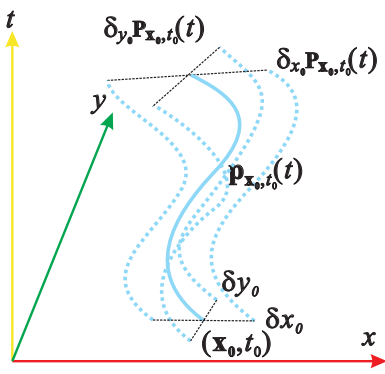
Figure 1: Lyapunov exponent of finite-time path-line.

formal discussion of the theory of FTLE fields and LCS. [8] used graphics hardware for the direct visualization of FTLE and [23, 7] have proposed efficient algorithms to compute LCS. [24] compared the LCS with the traditional vector field topologies.

As trajectories of dynamical flow advection, path-lines have been studied and visualized frequently. [38] visualizes a number of carefully selected path-lines to get static representations of the dynamical flow. [34] considers a segmentation of the flow domain based on local properties of path-lines, while [29] generates the asymptotic topological separation structures for periodic 2D time-dependent vector fields. [36, 37] applied texture based visualization approaches to capture path-line characteristics. [28] introduced an information visualization approach to explore the correlated structures of identified path-line attributes.

3 FLOW TRANSPORT VISUALIZATION

In flow dynamics it is critically important to see the patterns concerned with flow transport. However, most flow patterns are invisible to human perception. Flow visualization is the art of making the underlying patterns visible. A common way is to identify some visible distribution field related to flow motion and visualize the specified patterns through the corresponding distribution fields. The distribution fields are normally scalar fields either in 2D or 3D, which could be visualized in classical visualization approaches.

3.1 Path Line Integral Convolution

Line integral convolution (LIC) is one standard technique in flow visualization [5]. It imitates the motion blur of substance advection in a fluid whose results describe the substance concentration due to transport behavior of the fluid [27]. Classical LIC puts noise textures into a flow field and advects these textures along the flow transport. A visualization of the streamline structures can be obtained by observing the blurred result of the texture advection, which depict the geometrical distribution of transport trajectories .

Similarly, convolution along path-lines (Path-line LIC) provides an effective approach to uncover the dynamical information of flow transport [26].

Given a time-dependent vector field $\mathbf{v}(\mathbf{x},t)$, $\mathbf{x}$ describes the spatial component and t is the temporal component. We define a path-line $\mathbf{p}_{\mathbf{x}_0,t_0}(t)$ starting at $(\mathbf{x}_0,t_0)$, in the following way

$$\mathbf{p}_{\mathbf{x}_0,t_0}(t) = \mathbf{x}_0 + \int_0^t \mathbf{v}(\mathbf{p}_{\mathbf{x}_0,t_0}(\tau), \tau + t_0)\, d\tau \qquad (1)$$

A path-line is a function of time. It depends on the initial position $\mathbf{x}_0$, the initial time t_0 and the integration time t. A path-line integration can be carried out in both forward and backward direction. In real applications, flow data is usually given in a fixed spatial and

temporal domain, which means that we could only integrate path-lines for a finite-time. A path-line starting from $(\mathbf{x}_0,t_0)$ can be also parameterized in the form of $\mathbf{p}_{\mathbf{x}_0,t_0}(s)$ with a specific arc length s.

Given a scalar field, Path-line LIC consists of calculating a intensity value I by convoluting it along path-lines either for a fixed time:

$$I(\mathbf{x}_0,t_0) = \int_{-T_1}^{T_2} k(\tau) f(\mathbf{p}_{\mathbf{x}_0,t_0}(\tau), \tau)\, d\tau \qquad (2)$$

or for a fixed length:

$$I(\mathbf{x}_0,t_0) = \int_{-S_1}^{S_2} k(\tau) f(\mathbf{p}_{\mathbf{x}_0,t_0}(l), t(\mathbf{p}_{\mathbf{x}_0,t_0}(l)))\, dl \qquad (3)$$

where k denotes a filter kernel. $T_1 > 0$ and $T_2 > 0$ are the kernel lengths which specify the forward integration time and backward integration time. The integration could be restricted to one direction by simply setting the other parameter to 0. Similarly, $S_1 > 0$ and $S_2 > 0$ specify the integration arc length in forward and backward direction.

Note, in real applications, usually the resulting intensity is normalized by dividing either the total integration time or the integration arc length.

3.2 Lagrangian Coherent Structure

Lagrangian coherent structures (LCS) depict the transport barrier structures of the underlying flow processes. It could be precisely identified by a distribution field called finite-time Lyapunov exponent (FTLE) field [11].

The traditional Lyapunov exponent quantifies the asymptotic behavior of infinitesimally close particles in a dynamical system [18]. The Lyapunov exponent of a finite-time path-line is a finite-time average of the maximum expansion rate for a pair of particles advected in the flow. Consider a perturbed point $\mathbf{x}_0' = \mathbf{x} + \delta\mathbf{x}_0$ as shown in Fig. 1, where $\delta\mathbf{x}_0$ is infinitesimal. After a time interval t, this perturbation becomes $\delta_{\mathbf{x}_0}\mathbf{p}_{\mathbf{x}_0,t_0}(t) = \mathbf{p}_{\mathbf{x}_0',t_0}(t) - \mathbf{p}_{\mathbf{x}_0,t_0}(t)$. A linear flow map $A = \nabla_{\mathbf{x}_0}\mathbf{p}_{\mathbf{x}_0,t_0}(t)$ is computed to characterize the stretching gradient of the perturbation. The Maximum stretching occurs when $\delta\mathbf{x}_0$ is chosen such that it is aligned with the eigenvector associated with the maximum eigenvalue of $A^T A$. The maximum stretching is correspondingly the largest eigenvalue of $A^T A$. Through logarithm and normalization with the absolute advection time t, the definition of FTLE comes to

$$\delta_0^t(\mathbf{x}) = \frac{log(\sqrt{\lambda_{max}(A^T A)})}{t} \qquad (4)$$

A FTLE field of a dynamical flow provides an effective tool for characterizing LCS. Large FTLE values for forward advection correspond to unstable manifolds while large FTLE values for backward advection correspond to stable manifolds. For a FTLE field $\delta_{t_0}^t(\mathbf{x})$, LCS are defined as *ridges* of the field [10].

FTLE fields are able to capture the intrinsic transport behavior for general aperiodic systems where LCS can exist on a variety of time scales. This mechanism of capturing transport structures through identified attribute fields of path-lines provide a useful interface to characterizing inherent dynamical behavior of a flow and it can be extended for further analysis.

4 QUANTITY TRANSPORT STRUCTURE

Quantity transport is important and ubiquitous during a flow process. A fundamental question in the study of both turbulent and laminar mixing is the various transport phenomena such as material transport, energy transport or heat transport, as well as their interactions with each other. So it is important to comprehend the intrinsic characteristics of quantity transport during flow analysis. However,
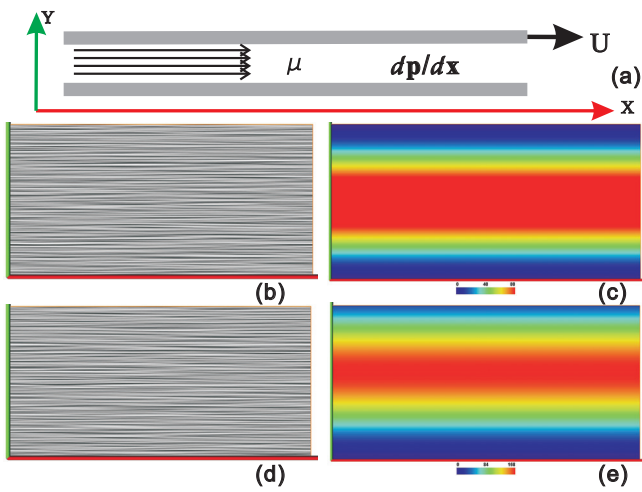
Figure 2: Visualization of a steady water flow between parallel plates: (a) Flow configuration; (b) Classical LIC visualization for $U = 0$; (c) Path-line LIC over kinetic energy field for $U = 0$; (d) Classical LIC visualization for $U = 8m/s$; (e) Path-line LIC over kinetic energy field for $U = 8m/s$.
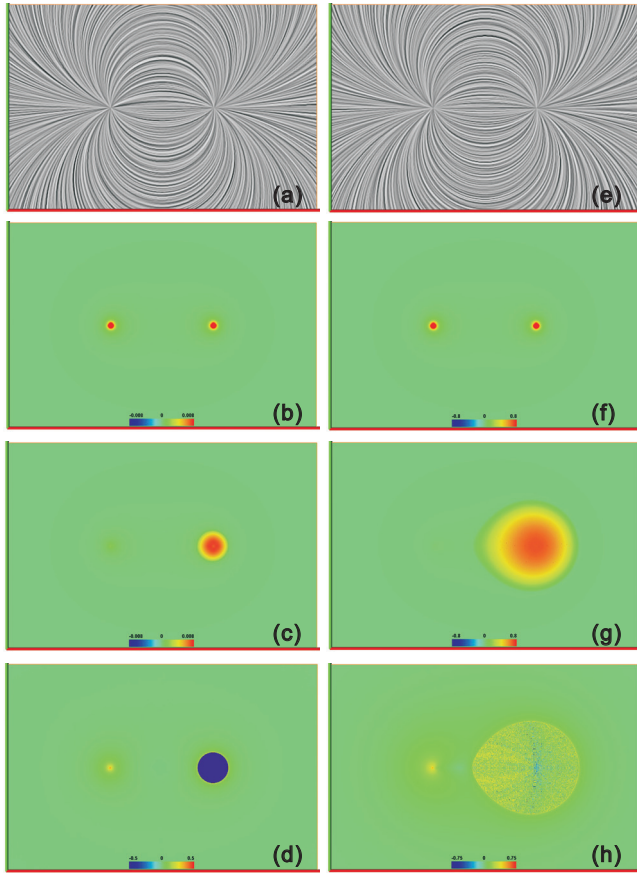
Figure 3: Visualization of a dipole flow, the left column $m = 0.0628$, the right column $m = 0.628$: (a,e) Classical LIC visualization; (b,f) Color coding of kinetic energy field; (c,g) Path-line LIC over kinetic energy field; (d,h) FTLE field.

the spatial-temporal complexity and the multi-mechanism nature make the understanding and visual analysis of these phenomena difficult and partially unsolved. We restrict our analysis to the advection behavior which is generally the dominant mechanism for flow quantity transport and use the motion blur technique to illustrate the transport nature.

4.1 Path-line LIC over Physical Quantities

To visualize intrinsic structures of quantity advection for flow fields, we also try to identify certain distribution fields concerning of flow motion. Convolution is a powerful tool to increase the visual depth into a complex phenomenon. It synthesizes motion blur of substance advection which provides an effective view to flow transport. Path-line integral convolution (Path-line LIC) is applied here to investigate the nature of dynamical transport of flow fields. Through Path-line LIC over certain field, we record the advection distribution of this field. A key step for Path-line LIC is to select proper quantity field for convolution. Classical approaches convolute noise textures to generate a motion blur field for visualization. However, this blurred result field after advection records only the information of geometrical distributions of either streamlines or path-lines. Some characteristic physical information is not well explored during the convolution. Instead of noise textures, we advect quantities of interest along flow fields and observe the advection distribution of the corresponding quantities, which reveals concentration nature of quantity transport.

A simple example is illustrated in figure 2 which describes an analysis over a well developed 2D water flow between two parallel plates. One plate is moving forward with certain velocity and the pressure gradient is constant for the flow (figure 2 a). This is a simple steady flow which can be well solved in flow dynamics [15]. Figure 2 b and d show a visualization using classical LIC approach for two cases with different plate moving velocities. We can see that the results are nearly the same. Geometrical distributions of transport trajectories are not enough to identify the full view of a dynamical behavior. The dynamical information, especially the structure nature of quantity transport, is also important during flow analysis. Instead of noise texture, we convolute the corresponding kinetic energy along path-lines and visualize the result distribution in figure 2 c and d. High values of this field indicate strong kinetic energy advections. This distribution uncovers the structures of the kinetic energy transport of this plate flow. The asymmetry of plate moving is clearly distinguished here.

Note that for steady flow, path-lines coincide with streamlines. We consider simple 2D steady flow in this section to illustrate some basic ideas.

An extension of LIC by color coding local properties [17] is used to supplement quantity information during flow transport. However, it still records the local information instead of the dynamical transport nature. Figure 3 shows an analysis of two dipole flow of different volume flow rate per unit depth m [15]. The first two rows show the comparison of the LIC visualization and color coding of local kinetic energy. Structurally, the visualization between the two dipoles are the same. The dynamical transport nature is not fully uncovered with either LIC or local quantity visualization. We apply Path-line LIC over local kinetic energy field and visualize the result distribution in figure 3 c and g. The values of the convoluted field indicate the advection magnitude and the high values point out the concentration trend of the underlying flow advection. Here, high values correspond to the sink area. These distributions reveal the advection nature of kinetic energy under the flow process. The inherent asymmetry is clearly observed in these kinetic energy transport structures. People can distinguish the two dipoles through the difference of the kinetic energy transport structures. Figure 3 d and h show the FTLE fields of corresponding dipoles which present the corresponding LCS. It is interesting that the kinetic energy trans-
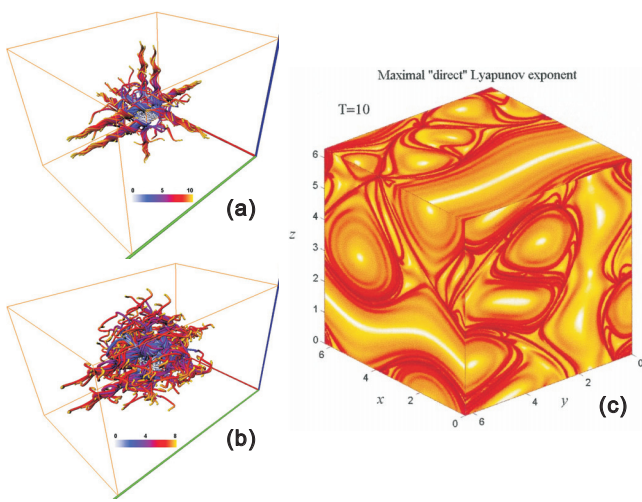
Figure 4: ABC flow: (a) Path-lines of steady ABC flow with integration time $T = 10$; (b) Path-lines of an unsteady ABC flow starting at $t = 0$ with integration time $T = 8$; (c)FTLE field of steady ABC flow [11].

Figure 5: Path-line LIC visulization of steady ABC flow: The left column visualizes the original quantity field; The right column visualizes the corresponding Path-line LIC result field.

port structures of dipole have some similarity with LCS appearing in the corresponding FTLE fields.

4.2 The Algorithm

Here we formulate the algorithm to visualize the finite-time transport structures for flow fields.

1. Identify the physical quantity of interest for investigation.

2. Pick up a certain time of interest and make a sampling in spatial domain.

3. Integrate path-lines from the sampling points in either forward or backward directions over a fixed time T.

4. Specify a convolution kernel and convolute the selected physical quantity field along path-lines.

5. Visualize the result field of the convolution and characterize the corresponding flow transport structures.

This algorithm needs some remarks:

To 1, this is the most important but flexible part of our approach. Conservative quantities should be considered to make sure the advection during the flow transport. We currently select those quantities which have been well applied in flow analysis. It could be also extended in future applications. There is no unique criteria for the selection, since different analysis in different applications may require different quantity fields. We provide users an interface for the further exploration.

To 2, we try to make the sampling resolution as high as possible to above the Nyquist frequency, however we need to balance our computation power. During our analysis, we use an adaptive mechanism, if we find some interesting areas, we will zoom into that area with a higher sampling resolution.

To 3, in our approach, we consider only finite-time path-lines. The path-line integration is carried out in one direction within a fixed time T. We use $T > 0$ for the forward integration and $T < 0$ for the backward integration. Our approach shares the same problem as other finite-time approaches on the setting of *integration time* for path-lines. It is a tradeoff between the fact that we want to have the path-lines to be analyzed as long as possible and the property that most of the path-lines should be integrated over the
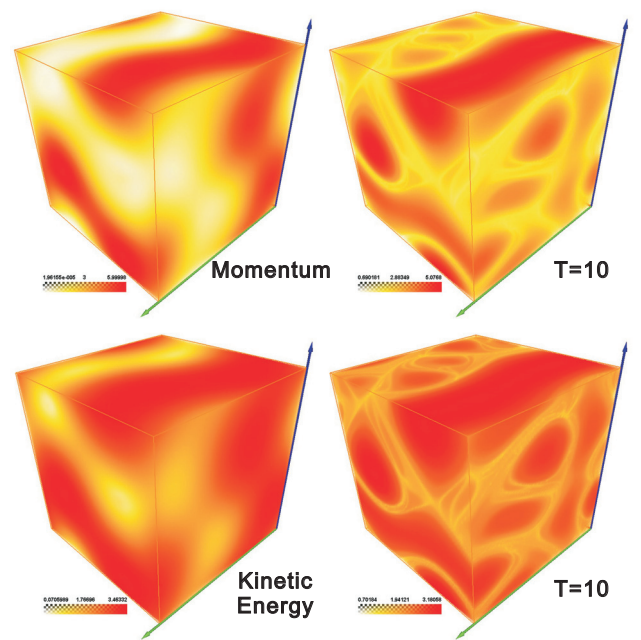
same time without leaving the domain. We have carefully set the integration time during our applications. However, to the best of our knowledge, there is still no guarantee of the optimization of the integration time setting. We use 4th order Runge-Kutta integration for the path-line integration.

To 4, we currently consider a simple box kernel [27] in our applications and restrict the analysis on the advection phenomenon of quantity transport. Diffusion or radiation analysis may be added by modifying the convolution kernel.

To 5, typical scalar visualization techniques can be chosen for the visualization of convolution result fields. In this paper, standard direct volume rendering and color coding are applied.

5 APPLICATIONS

We applied our approach to a number of data sets. In our current applications, we consider only the physical quantities such as momentum or kinetic energy for convolution, which are well-known for the transport in a flow. Nevertheless, we can also identify several interesting flow transport structures from these convoluted quantities which seem to hold even for different data sets.

Throughout this paper, we use a temperature color coding to characterize the time information along path-lines. We use the color red, green and blue to denote the x, y and z axis and yellow to denote the time axis in 2D time-dependent case.

5.1 ABC Flow

Figures 4 - 7 present results of analyzing two ABC (Arnold-Beltrami-Childress) flow fields

$$\mathbf{v}(\mathbf{x},t) = \begin{pmatrix} A\sin z + C\cos y \\ B\sin x + A\cos z \\ C\sin y + B\cos x \end{pmatrix} \quad (5)$$

where we set $A = \sqrt{3}, B = \sqrt{2}, C = 1$ for steady case and $A = \sqrt{3} + 0.5t\sin(2\pi t), B = \sqrt{2}, C = 1$ for unsteady case. This flow describes a solution of Euler's equation [13]. It is incompressible
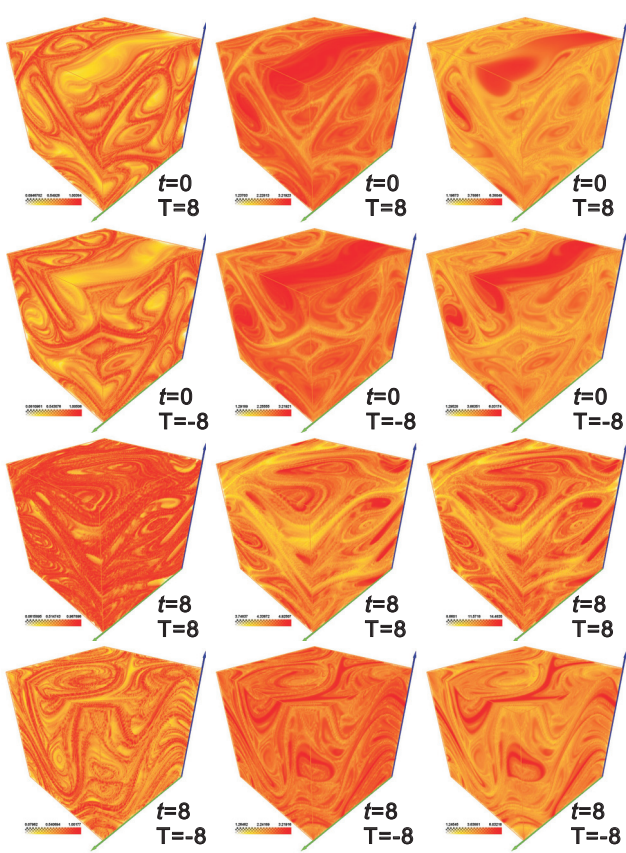
Figure 6: Path-line LIC visualizations of ABC unsteady flow: The left column visualizes the FTLE field starting at different t with different integration time T; The middle column visualizes the corresponding Path-line LIC convoluted field over local momentum field; The right column visualizes the Path-line LIC convoluted field over local kinetic energy field.

Figure 7: Path-line LIC visualization of generic fields. For each group, the upper visualizes the original field and the lower visualizes the corresponding Path-line LIC result. Group a and b test two random noise field; Group c-f test a normal function field $g(x,y,z)$ of different frequencies f.

and inviscid. We consider the spatial domain $D = [0, 2\pi]^3$ and used a sampling of $128 \times 128 \times 128$. Since this field is also defined outside the domain, we can integrate every path-line for a full time, even though it leaves the domain.

Figure 4 a shows some integrated path-lines for the steady ABC field with the integration time $T = 10$ while figure 4 b shows some integrated path-lines for the unsteady ABC field with the integration time $T = 8$. Figure 4 c is one visualization of the distribution of the FTLE fields of the steady ABC flow [11]. The corresponding LCS of the steady ABC flow can be visualized through this FTLE field. The upper left of figure 5 visualizes the local momentum field. We apply Path-line LIC over momentum and visualize the distribution in the upper right of figure 5. It is obvious to see the strong similarity between the transport structures presented in the Path-line LIC momentum field and the LCS. We observe that the local maximums in FTLE field corresponds to the local minimums in the Path-line LIC momentum field. It is not surprising that near LCS there is usually weak momentum advection. Similarly, the lower left of figure 5 shows the local kinetic energy field and the lower right of figure 5 shows the Path-line LIC kinetic energy field. We can observe the strong similarity again between the kinetic energy transport structure and the LCS.

In figure 6 we apply our approach to the unsteady ABC field and compared them with the classical FTLE fields. The left column of figure 6 visualizes FTLE fields computed at time $t = 0$ and $t = 8$ in forward and backward direction with the convolution time $T = 8$

and $T = -8$. LCS can be visualized through these FTLE fields. The corresponding distributions of Path-line LIC over momentum (middle column of figure 6) and kinetic energy (right column of figure 6) are visualized and the transport structures uncovered by these distributions present the same strong similarity with the corresponding LCS as the steady case.

We can see for both steady and unsteady ABC flow, either momentum or kinetic energy transport structures have significant similarity with the LCS. It is reasonable that in this ABC case, the flow transport is well behaved and structurally there is no difference between material transport, momentum transport or kinetic energy transport.

It is interesting that for ABC flow, if we apply our Path-line LIC approach over generic fields, we may also approach the structures which have some similarity to LCS though they have no obvious physical meaning. In figure 7, we apply our approach to different generic fields. Figure 7 a and b compare the results of Path-line LIC over two random noise fields while figure 7 c-f compare the results of Path-line LIC over $g(x,y,z) = sin^2(fx)sin^2(fy)sin^2(fz)$ with different frequency f. The LCS look-like structures appear when the dominant frequency of the generic fields approaching to the inherent frequency of ABC flow. It turns out that the concentration of generic substance advection tends to approaching the intrinsic structures of flow transport and the more correlation between a flow field and a quantity field, the better for Path-line LIC to uncover these intrinsic structures.
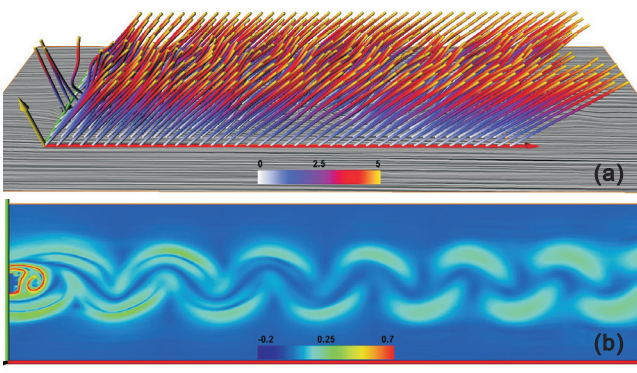
Figure 8: 2D dynamical cylinder flow: (a) Path-lines starting at $t = 0$ with integration time $T = 5$; (b) FTLE field.

5.2 2D Time-dependent Cylinder Flow

Figure 8 and 9 present some results of analyzing a 2D time-dependent flow behind a circular cylinder. The cylinder is put in the origin with radius 0.5. This is an incompressible laminar viscous flow [34]. The spatial domain of the data set is $[-9, 49.5] \times [-11, 11]$ and it is temporal periodic flow with one period $[0, 32]$. We focus the consideration on the area behind the cylinder ($[0, 28] \times [-3.5, 3.5]$) and make a sampling of 1000×250. For the result in the figures, we set an integration time $T = 5$. Figure 8a shows a visualization of some integrated path-lines starting at $t = 0$. Figure 8b shows a color coding of the corresponding FTLE field which visualizes the underlying LCS.

For the Path-line LIC, we also consider momentum and kinetic energy here. We convolute momentum and kinetic energy along path-lines and visualize them using color coding in figure 9 b and d. The original quantity fields are displayed in figure 9 a and c. We can see that the transport structures are significantly different from local structures. The low values of the Path-line LIC result field indicate weak flow advections. We can observe that the center area behind the cylinder has strong momentum or kinetic energy advection at the beginning while it turns to weak advection as the flow moves forward. Here we note that the momentum and kinetic energy transport structures presented in the Path-line LIC results have some similarities with the LCS at the areas near the location of the circular cylinder. The similarity decreases when the flow travels forward. This means that the momentum and kinetic energy advection have similar transport behavior with the material advection at the early stage and these quantity transport structures diffuse gradually as the increasing of the non advection effects during the flow transport. Compared the two quantity transport structures, we can also see that the momentum transport structures diffuse slower than the kinetic energy transport structures. It is interesting to compare the similarity or difference of various flow transport structures which contributes better understanding of the complex dynamical phenomena behind a flow.

5.3 Five Jet Flow

Figure 10 and 11 show an application of our approach on a 3D time-dependent flow which simulates five jets flying through a domain [6]. The spatial domain of the data set is $[0, 3.81m]^3$ and the temporal domain is $[0, 0.06s]$. The inflow velocity is $100m/s$. This data set is a compressible flow data for which the FTLE fields are not available for LCS. We focus our consideration on the center area ($[0.8m, 3.01m]^3$) where the jets fly through and make a sampling of $100 \times 100 \times 100$. The following result show two analysis starting at $t = 0.018s$ and $t = 0.024s$ with the integration time $T = 0.018s$ and $T = 0.024s$. Figure 10 a and b show some integrated path-lines
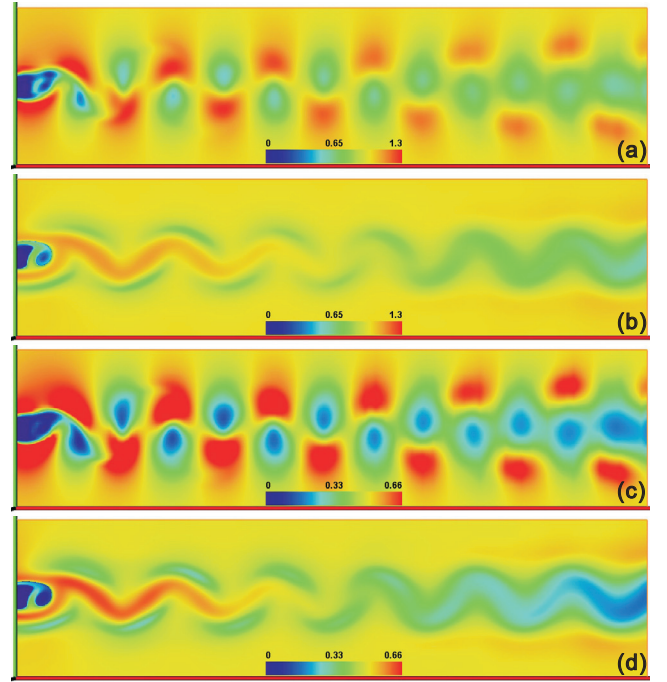
Figure 9: Path-line LIC visualization of 2D dynamical cylinder flow: (a) Local momentum field at $t = 0$; (b) Path-line LIC over momentum field starting at $t = 0$ with integration time $T = 5$; (c) Local kinetic energy field $t = 0$; (d) Path-line LIC over kinetic energy field starting at $t = 0$ with integration time $T = 5$.

with the integration time $T = 0.024s$.

The first column of figure 11 shows a Path-line LIC visualization of the density field starting at $t = 0.018s$. The upper visualizes the local density field at the starting time. The middle and lower visualize the Path-line LIC result fields with the integration time $T = 0.018s$ and $T = 0.024s$. The structures appeared in the Path-line LIC density result show the structure nature of the mass transport in the flow. The high value area of the result field indicates the region with strong mass advection which describes the trend of mass concentration while the low value area of the result field indicates the region of weak mass advection and the possible separation of mass advection. We can see that these mass transport structures present significant different information than the original local quantity field and depend little on the integration time when it is integrated long enough to uncover the structure. It is notable that even in a symmetric local setting, the underlying mass trans-
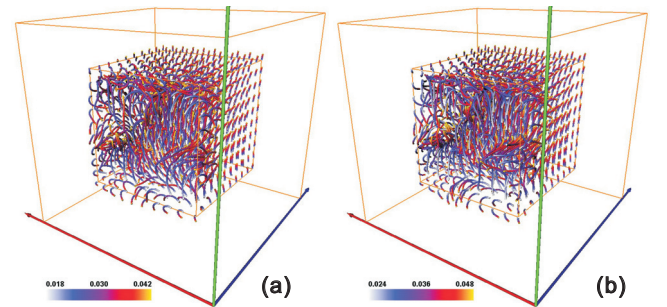
Figure 10: Path-lines of five jet flow starting at $t = 0.018s$ and $t = 0.024s$.
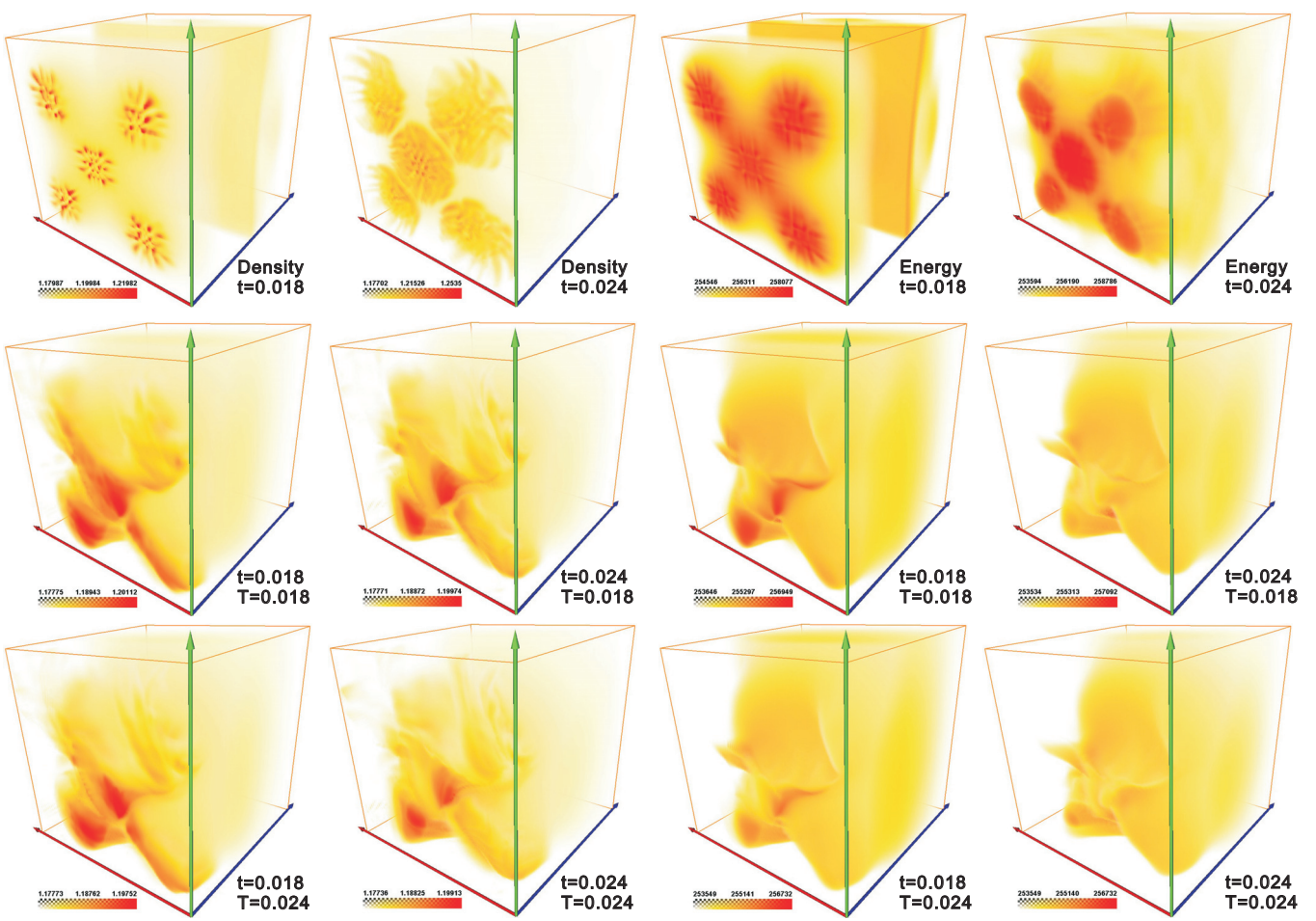
Figure 11: Path-line LIC visualization of five jet flow: The upper visualizes local density field at starting time; The middle visualizes the corresponding Path-line LIC result with $T = 0.018s$; The lower visualizes the corresponding Path-line LIC result with $T = 0.024s$.

port may behave asymmetrically [15, 16]. Similarly the second column show a Path-line LIC analysis of the density field starting at $t = 0.024s$. We can see again that the mass transport structures differ significantly from local quantity structures and depend little on the integration time. The asymmetry turns out again during the underlying mass advection. We can also observe some coherency between the two groups of transport structures and these structures reflect the intrinsic transport behavior of the underlying mass advection.

In the third and fourth column of figure 11, we apply our Path-line LIC approach to the corresponding energy field of the five jet data set. The structures appearing in the Path-line LIC result field figure out the underlying energy transport behavior. The high value area of the result field indicates the trend of energy concentration while the low value area of the result field indicates weak energy advection and the possible separation of the underlying energy advection. These energy transport structures are inherently asymmetric though the local field is symmetric. They have some coherency and depend weakly on the integration time. Through these structures, we can observe the intrinsic transport behavior of the underlying energy advection.

It is interesting to observe the difference between the mass transport structures and the corresponding energy transport structures. The visualization and comparison of different transport structures significantly improve the understanding of the complex phenomena of dynamical flow transport.

6 CONCLUSIONS

To getting insights into the transport behavior of dynamical processes is still a challenging problem. Quantities or trajectories provide separate view points towards the dynamical information. Our approach did a trial to combine the quantity analysis and trajectory analysis, and offers a higher level structure view of the dynamical behaviors underlying flow transport. This combination is constructed from the convolution over physical quantity fields along path-lines. In particular, we made the following contributions:

- We introduced an idea to convolute a correlated physical quantity field along finite-time path-lines.

- We proposed an approach to identify the finite-time flow transport structures for physical quantities.

- We applied our approach to a number of data sets and present some new insights into the dynamical behaviors.

However, we are not able to achieve accuracy in both the static information space and the dynamic information space. The observation of dynamical behaviors may come to the reduction of static details or even loss of some information. Nevertheless, these dynamical information presents different intrinsic view into the transport phenomena and contributes significantly to visual understanding of flow dynamics. Besides, in this paper, we only focus on the

visual analysis of the underlying transport structures, the theoretical analysis or proof is beyond our scope. For the future work, we could consider the variant of convolution kernels to include the analysis of non advection transport behaviors. For our computation, we haven't considered any acceleration algorithm for the convolution. It is worth doing a further acceleration for interactive application.

REFERENCES

[1] D. Banks and B. Singer. Vortex tubes in turbolent flows: Identification, representation, reconstruction. In *Proc. IEEE Visualization '94*, pages 132–139, 1994.

[2] D. Banks and B. Singer. A predictor-corrector technique for visualizing unsteady flow. *IEEE Transactions on Visualization and Computer Graphics*, 1(2):151–163, 1995.

[3] D. Bauer and R. Peikert. Vortex tracking in scale space. In *Data Visualization 2002. Proc. VisSym 02*, pages 233–240, 2002.

[4] R. B. Bird, W. E. Stewart, and E. N. Lightfoot. *Transport Phenomena*. John Wiley & Sons, 2001.

[5] B. Cabral and L. Leedom. Imaging vector fields using line integral convolution. *Computer Graphics*, 27:263–272, 1993.

[6] N. Fout, K.-L. Ma, and J. Ahrens. Time-varying multivariate volume data reduction. In *Proc. ACM Symposium on Applied Computing*, pages 1224–1230, March 2005.

[7] C. Garth, F. Gerhardt, X. Tricoche, and H. Hagen. Efficient computation and visualization of coherent structures in fluid flow applications. *IEEE Transactions on Visualization and Computer Graphics*, 2007.

[8] C. Garth, G. Li, X. Tricoche, C. D. Hansen, and H. Hagen. Visualization of coherent structures in transient flow. In *TopoInVis 07*, 2007.

[9] C. Garth, X. Tricoche, and G. Scheuermann. Tracking of vector field singularities in unstructured 3D time-dependent datasets. In *Proc. IEEE Visualization '04*, pages 329–336, 2004.

[10] G. Haller. Finding finite-time invariant manifolds in two-dimensional velocity fields. *Chaos*, 10(1):99–108, 2000.

[11] G. Haller. Distinguished material surfaces and coherent structures in three-dimensional fluid flows. *Physica D*, 149:248–277, 2001.

[12] G. Haller. Lagrangian coherent structures from approximate velocity data. *Physics of Fluids*, 14:1851–1861, 6 2002.

[13] G. Haller. An objective definition of a vortex. *J. Fluid Mech.*, 525:1–26, 2005.

[14] G. Haller and G. Yuan. Lagrangian coherent structures and mixing in two-dimensional turbulence. *Physica D*, 147(3-4):352–370, 2000.

[15] P. K. Kundu and I. M. Cohen. *Fluid Mechanics*. Academic Press, 2004.

[16] L. D. Landau and E. M. Lifshitz. *Fluid Mechanics*. Butterworth-Heinemann, 1987.

[17] R. S. Laramee, H. Hauser, H. Doleisch, B. Vrolijk, F. H. Post, and D. Weiskopf. The state of the art in flow visualization: Dense and texture-based techniques. *Comput. Graph. Forum*, 23(2):203–222, 2004.

[18] A. M. Liapunov. *Stability of Motion*. Academic Press, New York, 1966.

[19] K.-L. Ma. Visualizing time-varying volume data. *Computing in Science & Engineering*, 5(2):34–42, Mar. 2003. UCD.

[20] W. Merzkirch. *Flow Visualization*. Academic Press, 1974.

[21] A. C. Poje and G. Haller. Geometry of cross-stream lagrangian mixing in a double gyre ocean model. *J.Phys.Oceanogr.*, 29:1649–1665, 1999.

[22] C. Rezk-Salama, P. Hastreiter, C. Teitzel, and T. Ertl. Interactive exploration of volume line integral convolution based on 3D-texture mapping. In *Proc. IEEE Visualization '99*, pages 233–240, Washington - Brussels - Tokyo, Oct. 1999. IEEE.

[23] F. Sadlo and R. Peikert. Efficient visualization of lagrangian coherent structures by filtered amr ridge extraction. 2007.

[24] F. Sadlo and R. Peikert. Visualizing lagrangian coherent structures and comparison to vector field topology. *IEEE Transactions on Visualization and Computer Graphics*, 13(6), 2007.

[25] S. C. Shadden, F. Lekien, and J. E. Marsden. Definition and properties of lagrangian coherent structures from finite-time lyapunov exponents in two-dimensional aperiodic flows. *Physica D*, 212:271–304, 12 2005.

[26] H. Shen and D. Kao. Uflic - a line integral convolution algorithm for visualizing unsteady flows. In R. Yagel and H. Hagen, editors, *Proc. IEEE Visualization '97*, pages 317–323, 1997.

[27] H.-W. Shen, C. R. Johnson, and K.-L. Ma. Visualizing vector fields using line integral convolution and dye advection. In *Proc. Symposium on Volume Visualization*, pages 63–70, New York, Oct. 1996. ACM Press.

[28] K. Shi, H. Theisel, H. Hauser, T. Weinkauf, K. Matkovic, H.-C. Hege, and H.-P. Seidel. Path line attributes - an information visualization approach to analyzing the dynamic behavior of 3d time-dependent flow fields. In *TopoInVis 07*, 2007.

[29] K. Shi, H. Theisel, T. Weinkauf, H. Hauser, H.-C. Hege, and H.-P. Seidel. Path line oriented topology for periodic 2D time-dependent vector fields. In *Data Visualization 2006. Proc. EuroVis '06*, pages 139–146, 2006.

[30] D. Stalling and H. Hege. Fast and resolution independent line integral convolution. *ACM Siggraph '95*, pages 249–256, 1995. Los Angeles.

[31] D. Stalling, M. Westerhoff, and H.-C. Hege. Amira: A highly interactive system for visual data analysis. *The Visualization Handbook*, pages 749–767, 2005.

[32] H. Theisel, J. Sahner, T. Weinkauf, H.-C. Hege, and H.-P. Seidel. Extraction of parallel vector surfaces in 3d time-dependent fields and application to vortex core line tracking. In *Proc. IEEE Visualization '05*, pages 631–638, 2005.

[33] H. Theisel and H.-P. Seidel. Feature flow fields. In *Data Visualization 2003. Proc. VisSym 03*, pages 141–148, 2003.

[34] H. Theisel, T. Weinkauf, H.-C. Hege, and H.-P. Seidel. Topological methods for 2D time-dependent vector fields based on stream lines and path lines. *IEEE Transactions on Visualization and Computer Graphics*, 11(4):383–394, 2005.

[35] X. Tricoche, T. Wischgoll, G. Scheuermann, and H. Hagen. Topology tracking for the visualization of time-dependent two-dimensional flows. *Computers & Graphics*, 26:249–257, 2002.

[36] D. Weiskopf, G. Erlbacher, and T. Ertl. A Texture-Based Framework for Spacetime-Coherent Visualization of Time-Dependent Vector Fields. In *Proc. IEEE Visualization '03*, pages 107–114, 2003.

[37] D. Weiskopf, F. Schramm, G. Erlbacher, and T. Ertl. Particle and Texture Based Spatiotemporal Visualization of Time-Dependent Vector Fields. In *Proc. IEEE Visualization '05*, 2005.

[38] A. Wiebel and G. Scheuermann. Eyelet particle tracing - steady visualization of unsteady flow. In *Proc. IEEE Visualization '05*, page 77, 2005.